Ab initio study of early stages of III-V epitaxy on high-index surfaces of group-IV semiconductors: In adsorption on Si(112)

Hendrik Bentmann, John Houser, and Alexander A. Demkov*
Department of Physics, The University of Texas at Austin, Austin, Texas 78712, USA
(Received 9 May 2009; published 19 August 2009)

We consider theoretically the early stages of the epitaxy of III-V compound semiconductors on high-index surfaces of elemental semiconductors. Specifically, we compare two models for the 7×1 indium-induced reconstruction of the silicon (112) surface. Density functional theory calculations suggest a substitutional model to be favorable when compared to on-terrace step edge adsorption in good agreement with recent low-electron-energy diffraction and scanning tunneling microscopy experiments. In addition, we report a comprehensive study of the atomic reconstruction and electronic structure of the (112) surfaces of group-IV semiconductors diamond, silicon, germanium, and α-tin. We find the 1×1 rebonded reconstruction to be most stable for Si. For Ge and Sn the 2×1 reconstruction is most stable, and for carbon diamond it is 2×2. However, in all cases the mechanism of reconstruction is surprisingly similar to that known for the (001) surface.

DOI: 10.1103/PhysRevB.80.085311 PACS number(s): 68.35.B−

I. INTRODUCTION

As silicon-based complementary metal-oxide semiconductor (CMOS) technology has reached its fundamental materials limits, alternative channel materials offer a practical way to extend Moore's law beyond silicon. III-V materials, such as GaAs or InSb as well as other compound semiconductors with their very high carrier mobility, are now being considered as potential candidates for a channel material in future CMOS-type devices.[1,2] The most promising route to incorporate these advanced materials into CMOS is by growing epitaxial thin films on Si, either directly or *via* a buffer layer.[3] The direct growth by molecular beam epitaxy (MBE) on Si(001) is, however, not without its difficulties. Along with the usual lattice mismatch one has to solve an additional problem of orthogonal domains. In practice all semiconductor surfaces are *vicinal* or cut slightly off the crystallographic axis (typically by $\leq0.2°$). Thus the (001) surface of silicon, for example, consists of terraces separated by a single atomic step. Each terrace is 2×1 reconstructed with the rows of dimers running at 90° to one another on each consecutive terrace. During the MBE growth this 90° rotation results in formation of two orthogonal domains, which is highly undesirable. Growth on higher-index surfaces has been suggested to alleviate this problem.[4] While the low index surfaces as, e.g., the (001) and (111) surface of silicon or other group-IV semiconductors have been studied extensively, and are relatively well understood.[5] However, theoretical literature, in particular, focusing on the high index surfaces is sparse. One example is the (112) surface of silicon that has been successfully used for the epitaxial growth of II-VI compounds.[6–11] This surface is formed by facets with the (111) orientation, and therefore only twin domains can form. Several authors have also considered initial stages of III-V epitaxy, and several adatom reconstructions on Si(112) have been reported.[12–15] One case that has been studied in detail both experimentally and theoretically is the adsorption of gallium on Si(112).[15–17] It was found that gallium induces a 6×1 reconstruction where gallium atoms occupy step edge sites. Recently, Gai *et al.* performed scanning tunneling microscopy (STM) and low-electron-energy diffraction (LEED) studies of the indium-induced reconstruction of the Si(112) surface.[13] They report a quite different 7×1 reconstruction, and conclude that, unlike in the case of gallium, indium atoms do not segregate to the step edge sites. Instead they proposed a substitutional model. This is a rather important difference when one considers the kinetics of nucleation and growth. In general, the behavior of indium on Si surface is not very well understood. The early experimental studies of In adsorption on Si were performed on the (111).[18] The only theoretical work is a recent study of indium adsorption on the Si(100).[19] Understanding the reconstruction of the clean Si(112) is a critical first step to our understanding of the adatom adsorption. Density functional theory (DFT) is an ideal tool to investigate the early stages of epitaxy. It allows comparing different possible adatom arrangements on the basis of total energy and provides a clear picture of the electronic structure. Both can be directly compared to experiment.

The rest of the paper is organized as follows. First we briefly outline the computational methods used in this work. We then summarize the results of our comprehensive study of the clean (112) surface of diamond, silicon, germanium, and α-tin including surface energies, atomic and electronic structure, and work functions. We then discuss two recently proposed models for the indium-induced 7×1 reconstruction on the (112) surface of Si. We calculate the energy of adsorption, analyze the nature of bonding between indium and silicon, and compare our simulated STM images for both reconstructions with experiment. Based on the energetics and image comparison we conclude that the substitutional, and not the edge decorating model, is more plausible.

II. COMPUTATIONAL DETAILS

In our DFT (Ref. 20) calculations we employ projected augmented wave pseudopotentials[21,22] as implemented in the VASP code.[23] Exchange and correlation are treated within the

local-density approximation (LDA). The plane-wave expansions are restricted to cutoff energies of 400, 246, 288, and 241 eV for C, Si, Ge, and α-Sn, respectively. Integrals over the Brillouin zone are approximated by summing over special k points of the Monkhorst-Pack type.[24] Forces are calculated via the method of Hellmann and Feynman and minimized with the conjugate gradient method. The energy is converged to 10^{-6} eV/cell, and structures are relaxed until the forces on all atoms are less than 10 meV/Å. As a check we compute equilibrium lattice constants of 3.528, 5.402, 5.621, and 6.450 Å for C, Si, Ge, and α-Sn, respectively. The corresponding experimental values are 3.56, 5.43, 5.65, and 6.46 Å.[25] The overall agreement is very good. The surfaces are simulated using slab geometry by employing centrosymmetric cells that incorporate a slab of bulk material and a vacuum slab. The slabs for the clean surfaces are built of 17 layers of bulk material followed by at least 12 layers of vacuum in all calculations. We used $4\times4\times1$ k-point grids for the 2×1 reconstructions and $8\times4\times1$ k-points grids for 1×1 and 2×2 reconstructions. This choice of meshes allows for approximately equal density for different cells.

III. ATOMIC RECONSTRUCTION AND ELECTRONIC PROPERTIES OF THE (112) SURFACE

Several possible reconstructions of the Si(112) surface such as 4×2, 1×2, 1×1, and 2×1 have been reported in the literature on the basis of STM and LEED experiments.[26–34] In addition to these main reconstructions other STM experiments suggest the formation of (111) 7×7 and 5×5 nanofacets.[32,34] Most recent results by Fulk *et al.* strongly indicate that a $2\times$ reconstruction along the $[\underline{1}10]$ is always present.[35] The LEED patterns are typically very streaky along the $[\underline{11}1]$ direction indicating a complicated faceted reconstruction. Fulk *et al.* observed an increase in the facet size with the substrate temperature. Below 1150 °C rectangular LEED patterns occur. At higher temperatures additional hexagonal structures can be observed implying that the facet size has become large enough to accommodate a (111) 7×7 or 5×5 reconstruction. STM measurements by the same authors seem to confirm these observations.

Theoretical work on the clean Si(112) surface is rather scarce. Chadi and later Grein calculated surface energies and geometrical parameters for the 2×1 and the 1×1 rebonded (described below) reconstructions for silicon.[36–38] The electronic structure of the (112) surface of silicon has been only investigated for 1×1 models.[39,40] As far as we know this surface for other group-IV semiconductors has not been discussed in the literature.

In Fig. 1 we present the bulk-truncated (112) surface of the diamond crystal structure, common to group-IV semiconductors. The facetted nature of the surface is apparent. One also notes that atoms with one (C1 and C2) and two (A1) dangling bonds are present at the as-cut surface. In total, we find four dangling bonds per 1×1 surface unit cell. There exist two models for the ideal (112) surface. The first one results from perfect cleavage through the bulk material. In this model two edge atoms (A1 and A1′ in Fig. 1) form a dimer resulting in a 2×1 reconstruction. The number of dangling bonds is reduced to three per (1×1) unit cell. Another possibility is to simply remove these edge atoms. In this model atoms C1′ and C3′ form a dimer resulting in a 1×1 rebonded reconstruction. Here we end up with two dangling bonds per unit cell. However, the 1×1 rebonded reconstruction will impose more strain on the structure than the 2×1 reconstruction, possibly causing an energy increase. Both models are described in great detail by Chadi[35] and in the references in that paper. For silicon and carbon we also investigate a 2×2 reconstruction, where we repeated two 2×1 reconstructed unit cells with alternating dimer positions.

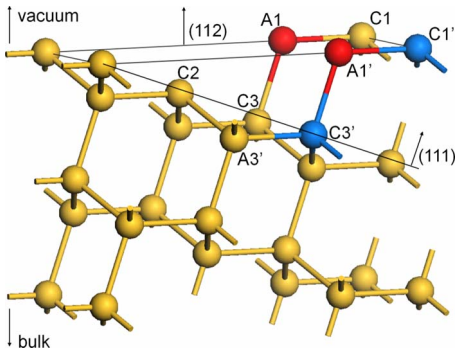

FIG. 1. (Color online) Ball and stick model of the ideal (112) surface. In the first model the edge atoms A1 and A1′ form a dimer resulting in a 2×1 reconstruction. In a second model these atoms are removed and atoms C1 and C3 form a dimer resulting in a 1×1 rebonded reconstruction.

All elements we consider exhibit a possible 2×1 reconstruction. The lengths of the dimers formed by the atoms A1 and A1′ for all elements are summarized in Table I. The larger the atom the longer is the dimer length in absolute numbers, and in terms of the interatomic distance in the respective bulk material. This behavior has also been observed for the 2×1 reconstruction of the (100) surface.[5] Note that the surface dimer in the case of carbon is shorter rather than longer than the equilibrium bulk bond length. Beyond the dimer formation we obtain further reconstructions driven by the relaxation of the remaining dangling bonds. These further reconstructions were not found by the authors in Refs. 36–38 which possibly accounts for a slightly lower surface energy for silicon in our calculation. While for silicon, germanium, and α-tin we obtain qualitatively the same reconstructions, carbon exhibits a totally different equilibrium structure. We will therefore discuss the case of carbon separately. In Fig. 2 we show a 2×2 section of the 2×1 reconstructed surface of

TABLE I. Dimer lengths for the 2×1 reconstructions of all elements in absolute units and in units of the interatomic distance in the bulk material.

	Dimer length in Å	Dimer length in units of the bulk bond length
Carbon	1.493	0.977
Silicon	2.379	1.017
Germanium	2.582	1.057
α-tin	2.973	1.064

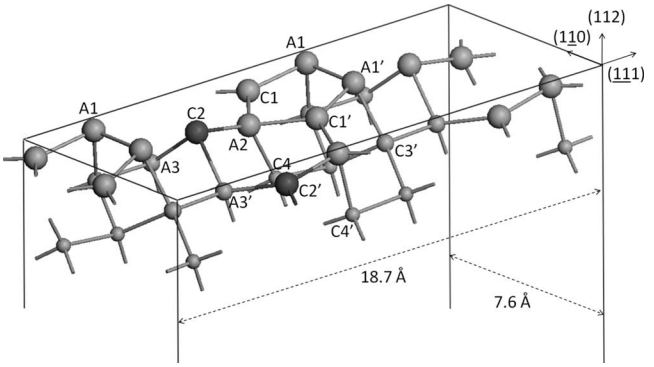

FIG. 2. Ball and stick model of the 2×1 reconstructed (112) surface of silicon. A 2×2 unit cell is shown for clarity. Atoms A1 and A1′ dimerize to reduce the dangling bond density to six per 2×1 unit cell. Atoms C1, C1′, and C2′ seek optimal positions for a sp^2 hybridization, i.e., they are almost located in plane with their bond partners and show increased bond angles near 120°. A contrary behavior is observed for atoms A1, A1′, and C2, where we find significantly decreased bond angles. This allows for the formation of energetically favorable *s*-like orbitals.

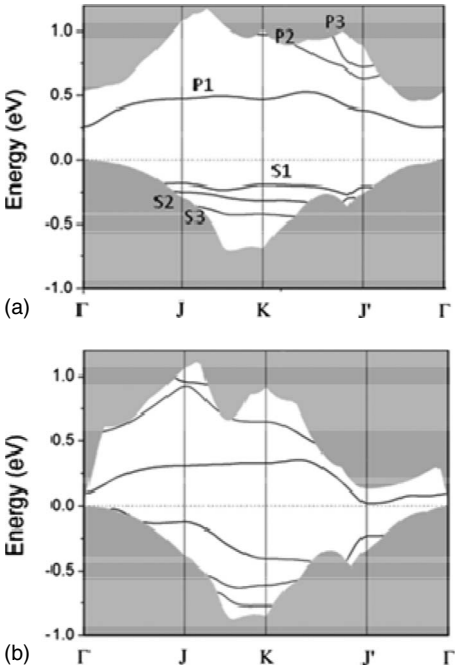

FIG. 3. Surface band structures of the 2×1 reconstructed (112) surface of (a) Si and (b) Ge. In both cases we find three occupied and three unoccupied surface bands in the fundamental band gap.

Si. A summary of important bond lengths and angles is presented in Table II. After the dimer formation between atoms A1 and A1′, there are six dangling bonds per 2×1 surface unit cell. Each of the atoms A1, A1′, C1, C1′, C2, and C2′ has one of them. We note that after the relaxation atoms C2′, C1, and C1′, on the one hand, are located nearly in one plane with their three neighbor atoms. Furthermore, their bond angles are increased from the ideal tetrahedral angle of 109.47° to values between 111.7° and 129.7°. We conclude that these three atoms try to find an optimal position for an sp^2 hybridization with bond angles of 120°. In the case of atom C2′ this is most obvious. Here, we find angles between 117.4° and 121.7°. According to this interpretation an unhybridized p-orbital remains at each of the three atoms. On the other hand, atoms C2, A1, and A1′ exhibit a completely different relaxation, most of the bond angles are decreased significantly below the value of 109.47°. Atom C2, for example, has bond angles between 94.6° and 99.8°. This is known as puckering, the dangling bond acquires more of the *s*-orbital character, which lowers its energy. This is very similar to the asymmetric dimer reconstruction of the Si(100) surface. Hence, per 2×1 surface unit cell we expect three energetically favorable *s*-like surface states, occupied by the six electrons (coming from dangling bonds), and three *p*-like unoccupied surface states.

In order to verify our interpretation of the atomic relaxation we now investigate the electronic structure of the surface. Figure 3 shows the surface band structures of Si and Ge along high symmetry lines in the 2×1 surface Brillouin zone. The well known underestimation of the band gap within the LDA is apparent. For silicon the band gap is about 0.5 eV and for germanium it is vanishingly small. In Fig. 3

TABLE II. Selected bond length and bond angles on the 2×1 reconstructed surface of Si.

Atoms	Bond length in units of the bulk bond length	Atoms	Bond angle in deg
A1 A1′	1.017	A1′ C1′ A2′	129.7
A1 C1	0.961	A2′ C1′ A2	113.2
A2 C1	0.981	A2′ C1′ A1′	116.9
A2 C2	0.989	A2′ C2′ A3	117.4
A2′ C2′	0.990	A3 C2′ A3′	121.8
C1′ A2′	1.002	A3′ C2′ A2′	117.5
C2 A3′	1.008	A2 C2 A3	94.6
A2 C4	1.055	A3 C2 A3′	99.2
A2′ C4′	1.022	A3′ C2 A2	94.7
		C3′ A1′ C1′	90.1
		C1′ A1′ A1	105.2

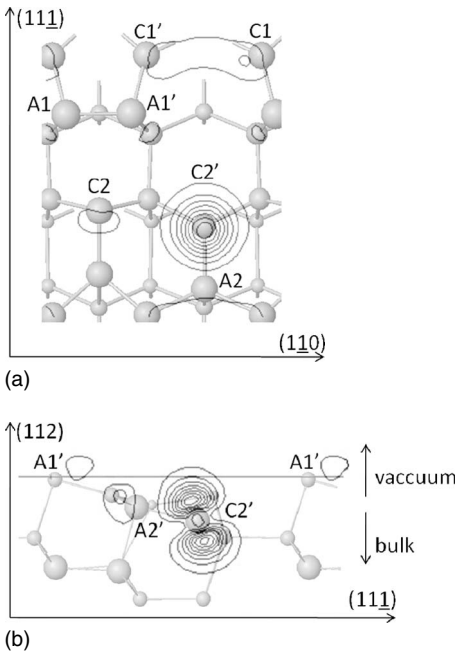

FIG. 4. Partial charge density of the lowest unoccupied band P1 [Fig. 3(a)] (a) in a plane perpendicular to the surface and (b) in a plane perpendicular to the (1$\underline{1}$0) direction. Atoms C2′ and A2′ are located in the plane of the contour plot in (b). Clearly, P1 band is a superposition of almost pure p_z states of the atoms C2′. Very small contributions from states at other surface atoms can be noted. Contours are scaling linearly between 0 and (a) 22 $me^-/Å^3$ and 96 $me^-/Å^3$.

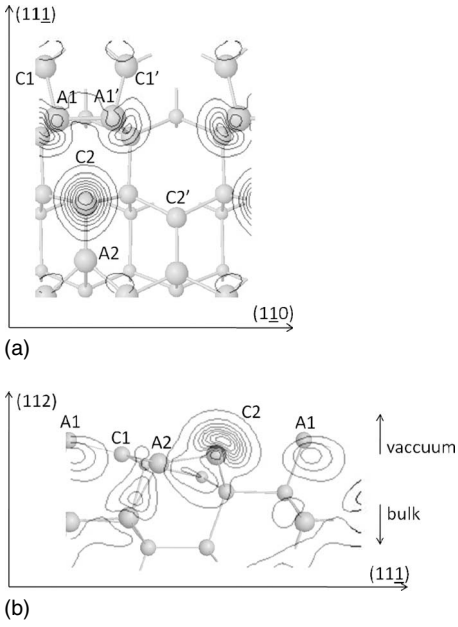

FIG. 5. Partial charge density of the highest occupied band S1 [Fig. 3(a)] (a) in a plane perpendicular to the surface and (b) in a plane perpendicular to the (1$\underline{1}$0) direction. Atoms C2 and A2 are located in the plane of the contour plot in (b). We note strong contributions from *s*-like dangling bond states at atoms C2, A1, and A1′. Due to the mixing of the band S1 with bulk states also small contributions from atoms in lower layers are apparent. Contours are scaling linearly between 0 and 42 $me^-/Å^3$ in (a) and (b).

we merely present the fundamental gap, which suffices for our purposes. The valence band top is set to zero energy. For both, Si and Ge, we find the surface in a semiconducting state. Three occupied surface bands are separated by a finite energy gap from three unoccupied bands in both cases. This is exactly what we expect from our qualitative considerations above. The analysis of the localization of these states provides a proof for our interpretation. We calculate the square of wave functions summed over all k points for a single surface band. This quantity is the partial charge density due to a particular band. In Fig. 4(a) we show the partial charge density of the lowest unoccupied surface band P1 of Si [see Fig. 3(a)] in a plane perpendicular to the (112) direction (top view). We note that this band is localized at atom C2′. Only very small contributions from other surface atoms are apparent. Figure 4(b) shows the same quantity in a (1$\underline{1}$0) plane (side view). Atoms C2′ and A2′ are located in the plot layer. Here it becomes clear that the P1 band is almost solely a superposition of atomic p_z states located at the atoms C2′. Similarly, we find the bands P2 and P3 in Fig. 3(a) to be mainly composed of p_z states at the atoms C1 and C1′. These findings confirm our interpretation of the atomic structure. Next we investigate the partial charge density due to the highest occupied surface band S1. It is shown in Figs. 5(a) and 5(b) where the contour plots are oriented in the same way as in Figs. 4(a) and 4(b). The atoms C2 and A2 are located within the plot layer of Fig. 5(b). We observe a strong localization of the partial charge density at the atoms C2, A1, and A1′. In contrast to Fig. 4(b) the *s*-like nature is apparent. Furthermore, we see a slight contribution to the bond between atoms A1 and A1′. Due to the resonant nature of the surface band S1 also small contributions from atoms in lower layers are present. We find bands S2 and S3 lying lower in energy, to have a very similar localization as band S1. They contribute slightly more charge than the band S1 to the bond between atoms A1 and A1′. We conclude that, in the case of Si, Ge and α-Sn, six dangling bonds per surface unit cell occupy mainly *s*-like states at atoms C2, A1, and A1′. At the same time p_z states at atoms C2′, C1, and C1′, remain unoccupied. This splitting of the surface bands lowers the surface energy additionally to the dimer formation.

As mentioned above, the 2×1 reconstruction of carbon differs qualitatively from that of the other elements. The equilibrium structure after the relaxation is shown in Fig. 6. A summary of important bond lengths and angles is given in Table III. We observe the formation of fivefold rings consisting of atoms A1, A1′, C1, C2′, and A2. All these atoms are nearly located in the top layer parallel to the surface. A rather unusual bond breaking between the atoms A2 and C4 can be noticed, enabling atom A2 to adopt its position within the ring. The bond angles within the ring (the first five values in Table III) are close to 108°, the angle in a perfect pentagon. The other angles between the bonds within the ring and those directed downward to atoms in the second or third layer are, with one exception, close to 120°. As a result the structure somewhat resembles that of the face of a C_{60} molecule. Additionally, we note three bonds between atoms A1 and C1, A1′ and C1′, as well as A2 and C2 to have a length of only 1.36 Å. This indicates the formation of double-bonded

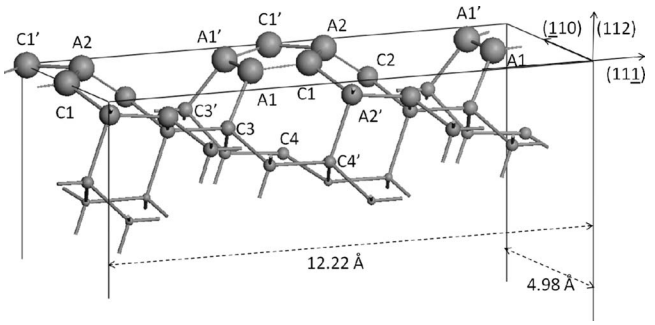

FIG. 6. Ball and stick model of the 2×1 reconstruction of the (112) surface of carbon. We observe the formation of fivefold rings after an unusual bond breaking between atoms A2 and C4.

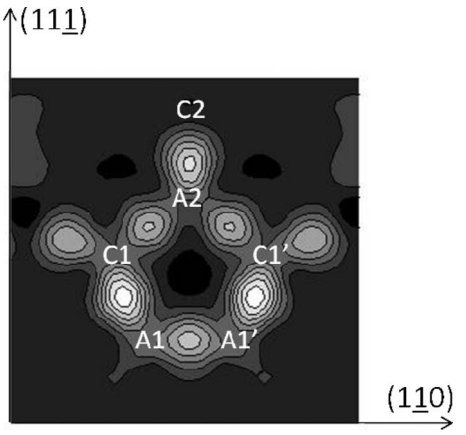

FIG. 7. Valence charge density difference between the calculated density and the charge density of free carbon atoms. The plot shows a section of the 2×1 surface unit cell that incorporates the fivefold ring of atoms that has formed after the relaxation. The larger (smaller) charge accumulations arise from double (single)-bonded dimers.

dimers, which often occur on carbon surfaces and molecules. The double—bond in a C_2H_4 molecule, for example, has a length of 1.34 Å. In Fig. 7 we present the valence charge density in a layer parallel to the surface. In order to emphasize the charge transfer in the region between the atoms, atomic valence charge densities are subtracted. The atoms are labeled as in Fig. 6. Double bonds are clearly visible as areas of charge accumulation when compared to single bonds. Further analysis of the surface electronic structure reveals that the Fermi energy is pinned by a surface state 1.5 eV above the valence band top.

We also determine the work functions for the 2×1 reconstructed surfaces for all elements using the reference potential method suggested by Kleinman.[41] As a reference we use the macroscopic average of the plane-averaged electrostatic potential.[42] The work function is given by

$$\phi = E_{vac} - E_F. \tag{1}$$

The vacuum energy E_{vac} is taken as the electrostatic potential value in the vacuum region of the slab. Table IV summarizes the values we obtained. To gauge the reliability of our calculation we also calculate the work function of the Si 2×1 reconstructed (100) surface, and obtain 5.11 eV in good agreement with the experimental value of 5.17 eV. Also for carbon using the experimental band gap of 5.47 eV we find a negative electron affinity of approximately −1.2 eV. A similar value of −0.8 eV has been reported for the 2×1 reconstructed (100) surface.[43]

We now briefly discuss the 1×1 rebonded reconstruction of silicon. The dimer formed by the atoms C1′ and C3′ (Fig. 1) has an equilibrium length of 2.517 Å (5.8% longer than the bulk bond length). Additionally, the bond between the atoms A3′ and C3′ is stretched to 2.608 Å (9.6% longer than the bulk bond length). The surface is found to be semiconducting. A doubly occupied surface state, mainly located at atom C1′, is observed. Similar to the 2×1 reconstruction, we find an unoccupied, p_z-like surface state at the atom C2.

IV. SURFACE ENERGY

Employing slab geometry, it is straightforward to calculate total surface energies. The slabs contain two equivalent surfaces, one at the bottom and one at the top. We determine the surface energies using the following equation:

TABLE III. Selected bond lengths and bond angles on the 2×1 reconstructed surface of C.

Atoms	Bond length in units of the bulk bond length	Atoms	Bond angle in deg
A1 A1′	0.977	A1 A1′ C1′	109.2
A1 C1	0.892	A1′ C1′ A2	106.0
A2 C1	0.960	C1′ A2 C1	109.0
A2 C2	0.889	A2 C1′ A1	106.1
A2′ C2′	0.971	C1 A1 A1′	109.2
C1′ A2′	0.984	C1 A1 C3	118.7
C2 A3′	0.973	C3 A1 A1′	108.2
A2 C4	1.673	A2 C1 A2′	120.6
A2′ C4′	1.022	A1 C1 A2′	123.9
		C2 A2 C1	119.0

TABLE IV. Work functions of the 2×1 reconstructed (112) surface for all elements.

	Carbon	Silicon	Germanium	α-tin
Work function φ in eV	5.17	5.11	4.72	4.46

$$E_{surface} = \frac{1}{2A}(E_{slab} - NE_{bulk}), \quad (2)$$

Here A is the area of the surface unit cell, E_{slab} is the total energy of the slab, E_{bulk} is the energy per atom in the bulk material, and N is the number of atoms contained in the slab. The factor of $\frac{1}{2}$ accounts for two equivalent surfaces in the supercell. In Table V the surface energies resulting from all our calculations are summarized. Before we analyze our results in more detail we first comment on the chemical trend in the surface energies. The larger the band gap the higher is the surface energy. It also inversely correlates with the atom size, which can be easily understood for the gap scales roughly as the difference between the metallic and covalent energy (V_2-V_1). The first scales as the inverse of the interatomic distance, while the second is just the quarter of the s-p splitting which is almost constant for the entire group IV.[44] This trend has been discussed in the context of low index surfaces.[5]

For silicon the 1×1 rebonded reconstruction is the most stable configuration with a surface energy of 1.46 J/m^2. The lower dangling bond density of the 1×1 rebonded reconstruction wins against the lower strain energy of the 2×1 reconstruction with a surface energy of 1.56 J/m^2. In Ref. 5 we find calculated surface energies of 1.36 J/m^2 for (111) 7×7 and 1.45 J/m^2 for (100) 2×1. Our numbers agree well with previous results of Grein.[39] However, while for the 1×1 rebonded reconstruction we exactly reproduce Grein's result our value for the 2×1 reconstruction is about 2.5% lower. This difference might arise from the additional symmetry breaking found in our calculation as described in the last section. We estimate this decrease, additional to the dimer formation, to be 3.2 J/m^2 when we compare our result to that of Ref. 39. This should be compared to the energy difference between the symmetric and asymmetric dimer model of the Si(100) surface which is 2.24 J/m^2.[45] Our model for the 2×2 reconstruction does not exhibit any energy gain when compared to the 2×1 reconstruction.

In the case of carbon we find the 2×2 reconstruction to be the most stable configuration with a surface energy of 5.35 J/m^2. However, the 2×1 reconstruction is very close in energy. Interestingly, the 1×1 rebonded reconstruction is energetically very unfavorable (presumably due to the very stiff bonds in carbon). For comparison, previously calculated surface energies of carbon diamond are 4.06 J/m^2 for (111) and 5.71 J/m^2 for (100) 2×1.[5]

For germanium and α-Sn we find the 2×1 reconstruction to have the lowest energy with 1.15 and 0.66 J/m^2, respectively. For Ge we can compare our results for the (112) surface o previously calculated surface energies of 1.02 J/m^2 for (111) 7×7 and 1.05 J/m^2 for (100) 2×1.[5]

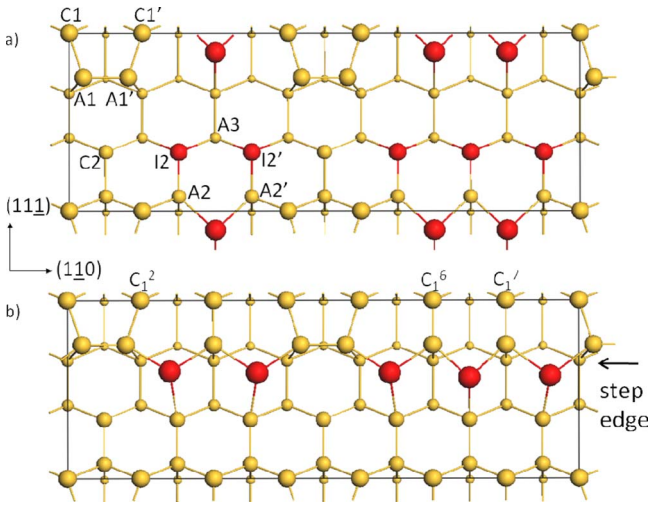

FIG. 8. (Color online) Ball and stick of the two models for the 7×1 indium-induced reconstruction of the silicon (112) surface. Indium atoms are marked with red color. (a) A substitutional model proposed by Gai *et al.* on the basis of STM and LEED experiments. (b) The step edge model. Indium atoms occupy sites at the step edge of the surface.

V. INDIUM INDUCED 7×1 RECONSTRUCTION OF THE SI(112) SURFACE

We shall compare two existing models for the 7×1 reconstruction. Both are shown in Fig. 8. In the first model [Fig. 8(a)] certain surface silicon atoms are replaced by indium atoms. This model describes a substitutional adsorption where indium atoms kick out silicon atoms and take their places. This model was proposed by Gai *et al.* on the basis of their STM and LEED experiments and is described in more detail in Ref. 13. However, our model differs slightly from the one introduced by Gai *et al.* In their model the indium atom in the upper right corner of the 7×1 surface unit cell in

TABLE V. Total surface energies for all considered elements and reconstructions in J/m^2.

	1×1 unrelaxed	1×1 relaxed	1×1 rebonded	2×1	2×2
Carbon	8.21	6.53	6.53	5.37	5.35
Silicon	2.15	1.72	1.46	1.56	1.57
Germanium	1.66	1.21	1.18	1.15	
α-tin	1.01	0.72		0.66	

Fig. 8(a) remained a silicon atom that was not substituted. Our STM simulations show that this silicon atom would cause a bright spot that cannot be found in the experimental data. The second model is the step edge model, which was introduced to describe the gallium induced 6×1 reconstruction of the Si(112) surface. The step edge model describes an on-surface adsorption with only minor geometrical changes in the substrate. We perform slab calculations for both models. The slabs are built of 11 layers of bulk material and 11 vacuum layers, resulting in 176 (a) and 192 (b) atoms per supercell. The dimensions of the supercells are $26.7\times9.4\times26$ Å^3. The structures are relaxed until the forces on all atoms are less than 20 meV/Å. The electronic relaxation is performed up to an accuracy of 10^{-6} eV/cell and we use $2\times4\times2$ k-point grids.

First we determine adsorption energies for both models. For the on-surface adsorption in the step edge model we define the adsorption energy according to the following equation:

$$E_{ads} = -\frac{1}{Q}[E_{\mathrm{In/Si}} - E_{substrate} - N_{\mathrm{In}}(E_{atom,\mathrm{In}} + \mu_{\mathrm{In}})], \quad (3)$$

where $E_{\mathrm{In/Si}}$ is the total energy of the slab including the adsorbed indium atoms, $E_{\mathrm{atom,In}}$ is the energy of a free indium, μ_{In} is the chemical potential of indium, N_{In} is the number of indium atoms in the slab, and $E_{\mathrm{substrate}}$ is the total energy of the clean surface, which we defined as two 2×1 reconstructed surface unit cells and three 1×1 relaxed surface unit cells building up the 7×1 unit cell. The way we defined μ_{In} in (3), $\mu_{\mathrm{In}}=0$ corresponds to exchange with free indium atoms. Q is a normalization factor that equals either the number of indium atoms in the slab or twice the area of the surface unit cell. Then E_{ads} is either the averaged adsorption energy per adsorbed atom or the adsorption energy per surface unit area, respectively.

For the substitutional model we use the following equation to define the adsorption energy:

$$E_{ads} = -\frac{1}{Q}[E_{\mathrm{In/Si}} - E_{substrate} - N_{\mathrm{In}}(E_{atom,\mathrm{In}} + \mu_{\mathrm{In}}) + N_{\mathrm{Si}}E_{Bulk,\mathrm{Si}}], \quad (4)$$

where we use the same definitions as in Eq. (3). The last term accounts for silicon atoms that are kicked out during the adsorption process. These atoms are assumed to rebound at kink sites at steps and regain the bulk cohesive energy. Equations (3) and (4) are commonly used to define adsorption energies.[46] In Fig. 9 we show the adsorption energy per surface unit area as a function of μ_{In}. We note that in the regime between $\mu_{\mathrm{In}}=0$ and $\mu_{\mathrm{In}}=-2.45$ eV the substitutional model is energetically favorable. In the regime where $\mu_{\mathrm{In}}<-2.45$ eV the step edge model provides the higher adsorption energy. We find the substitutional model to have considerably higher adsorption energy under the indium rich conditions corresponding to $\mu_{\mathrm{In}}\approx0$. Table VI summarizes the energies for $\mu_{\mathrm{In}}=0$.

In order to relate our calculations to the experimental results, we simulate STM images for both models. In the simplest approximation the intensity of an STM image is related

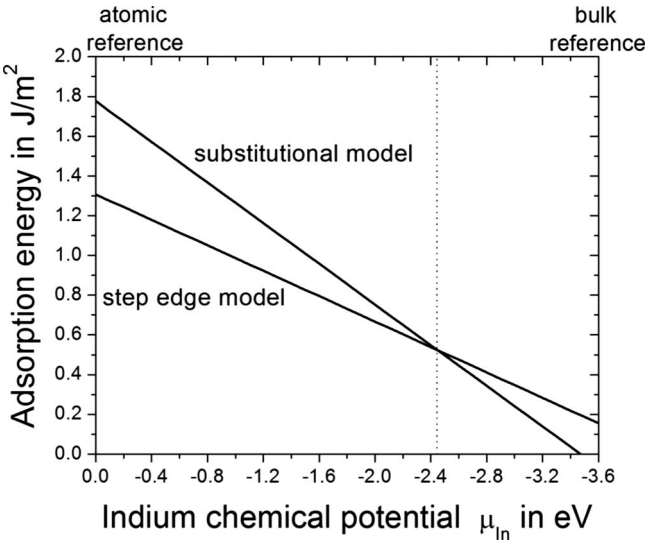

FIG. 9. Adsorption energy E_{ads} per surface unit area as a function of the indium chemical potential μ_{In} for the substitutional model [Fig. 8(a)] and the step edge model [Fig. 8(b)]. In the regime of $\mu_{\mathrm{In}}\approx0$ that reflects the experimental conditions the substitutional model exhibits the higher adsorption energy.

to the local density of states (LDOS) of the sample material at the tip position, integrated over the energy range given by the voltage between the tip and sample.[47] One assumes the LDOS at the tip to be constant in the considered energy range. We only consider zero temperature, and consequently, the intensity is given by

$$I(\vec{r}) = \sum_{\substack{n,\vec{k} \\ E_F - eV < E_n(\vec{k}) < E_F}} |\varphi_{n,\vec{k}}(\vec{r})|^2, \quad (5)$$

where the $\varphi_{n,k}$ are the single particle solutions of the Kohn-Sham equations.

We estimate the distance between the tip and sample to be ~3 Å. Within reasonable deviations from this value the images are not sensitive to this parameter. Following the experiment we chose $V=-1.2$ V. Thus we are producing filled state images. The results are shown in Figs. 10(a) and 10(b). They have to be compared to Fig. 2(c) in Ref. 13. For the substitutional model in Fig. 10(a) we observe twofold oblong features mainly at atoms A1 and A1′. The oblong spots are slightly tilted against each other. Just like on the clean surface, occupied surface orbitals arise at atoms A1 and A1′. Consequently, atoms C1 and C1′ are hardly visible in the filled state image as their dangling bond orbitals are unoccupied. Perhaps more importantly, atoms A1 and A1′ are about

TABLE VI. Adsorption energies per surface area and per atom for model I and the step edge model ($\mu_{\mathrm{In}}=0$).

	Adsorption energy in J/m^2	Adsorption energy in eV/atom
Substitutional model	1.78	3.47
Step edge model	1.31	4.08

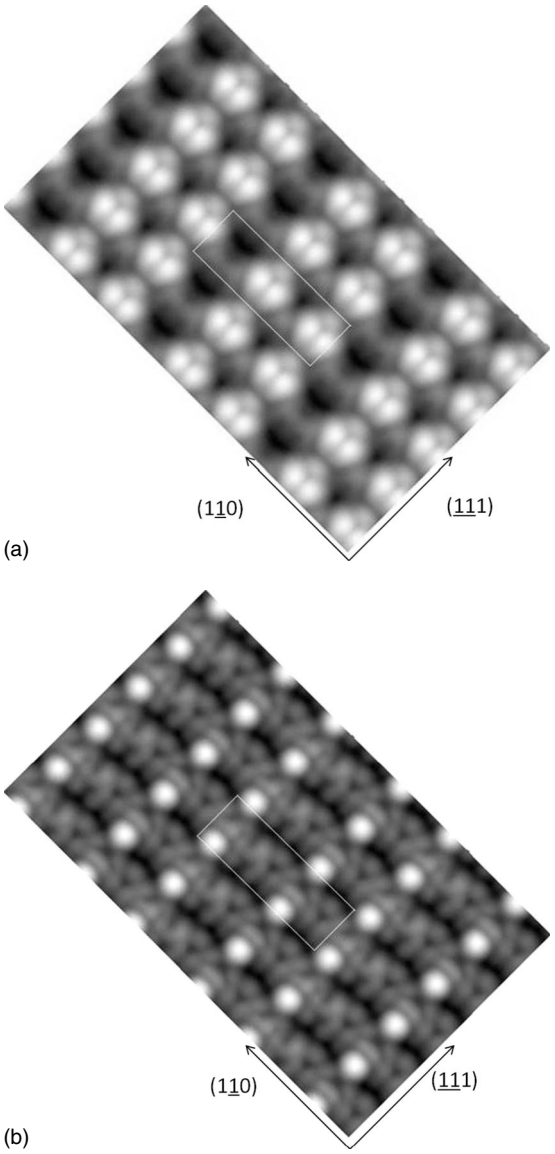

FIG. 10. Simulated STM images for the two models of the 7 $\times$1 indium-induced reconstruction of the Si(112) surface (logarithmic scale, details in text). The STM image corresponding to the substitutional model is shown in (a). We find good agreement with the experimental data of Gai and co-workers. In (b) we present the image corresponding to the step edge model. The images are rotated for convenient comparison with Fig. 2(c) in Ref. 3.

0.57 Å higher than atoms C1 and C1′ because of their downward relaxation as previously discussed. The tunneling current decays exponentially with the distance. These observations are in complete agreement with the experimental data of Gai *et al.* In our simulation the oblong spots are interrupted by a weaker spot between them. These weaker spots correspond to the silicon atoms C2. These spots are not observed in the experimental data and constitute the only drawback in our comparison. Furthermore, we find dark areas at the indium sites due to their positions between 0.57 and 1.3 Å below the uppermost Si atoms. This also corresponds well with the experimental STM image. Overall we find very good agreement between our simulations and the experimental data of Gai *et al.* in almost every important feature of the images. On the other hand, the image corresponding to the step edge model shows no similarity to the experimental results. Atoms A1 and A1′ are not visible anymore as they form an additional bond with the adsorbed indium atoms. We observe two very bright spots at atoms C_1^2 and C_1^7, which moved upward during the relaxation. We will not consider the step edge model in more detail as the disagreement with the experiment is obvious.

Summarizing our results so far, we note that the substitutional model is energetically favorable when compared to the step edge model. The simulated STM image of the substitutional model corresponds well to the experiment while that of the step edge model does not. We therefore conclude that the step edge model has to be ruled out for the 7 $\times$1 reconstruction, at least for the experimental conditions in Ref. 13. Overall, our results support the interpretation of Gai and coworkers in that the indium adsorption is substitutional. Further investigations will have to clarify the minor discrepancies between the experiment and our simulated STM images. In general, it should be noted that an STM image is not directly related to the atomic geometry at the surface but rather to the electronic structure at the surface near the Fermi level. Hence, there are always remaining ambiguities when deducing the geometric structure from STM measurements.[48,49] However, in our case the substitutional model is supported by phenomenological arguments[13] as well as by first-principled calculations.

The analysis of the DOS reveals the surface in the substitutional model to be semiconducting with a band gap of about 0.15 eV (within the LDA). We also observe a significant drop in the work function of 0.46 eV due to indium adsorption. Figure 11 shows the LDOS in the vicinity of the Fermi energy for the specific atoms in the slab. Si atoms in the middle of the slab, representing almost bulklike Si atoms make a relatively small contribution to the LDOS just below the Fermi energy. The states just below the Fermi energy in the energy window of 0.25 eV are mainly due to the adsorbed In atoms.

In Fig. 12 we present the charge density difference Δn between the charge density of the adsorbate system and the charge density of the clean substrate plus free indium atoms,

$$\Delta n = n^{\mathrm{In/Si}} - n^{substrate} - n^{\mathrm{In}/atom} \tag{6}$$

This quantity tells us about the actual charge transfer in the system during the adsorption process. Figure 12 displays a section of the complete 7 $\times$1 unit cell. Atoms are labeled as in Fig. 8(a). The light (dark) regions correspond to positive (negative) Δn. Three areas of positive Δn emerge at each indium atom, while almost spherical spots of negative Δn are found directly at the indium sites. We can readily identify the regions of positive Δn as three directional covalent bonds for each indium atom. Furthermore, we note that the peak in the charge density is closer to the silicon atoms as one should expect from the higher electronegativity of silicon compared to indium. We find bond lengths between indium and silicon atoms in the range of 2.49 and 2.56 Å.

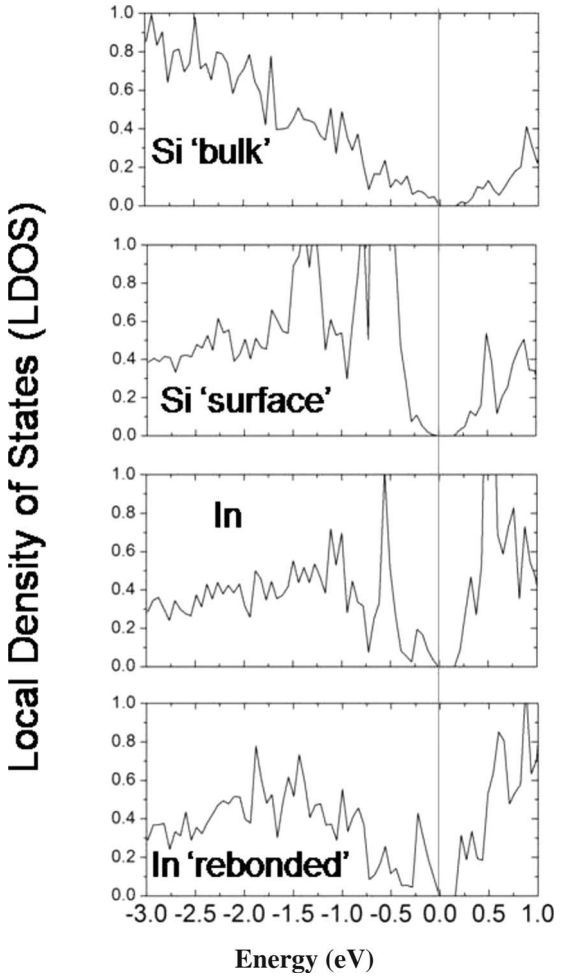

FIG. 11. The local density of states near the Fermi level (E_F =0 eV) probed at Si atoms in the middle of the slab (Si "bulk"), at the dimerizing Si atoms A1 (Si "surface"), at the In atoms In2 (In) and the rebonded In atoms (In "rebonded"). The surface is found to be semiconducting with a gap of about 0.15 eV. The states just below the Fermi level are identified to be mainly due to the In atoms. See text for details.

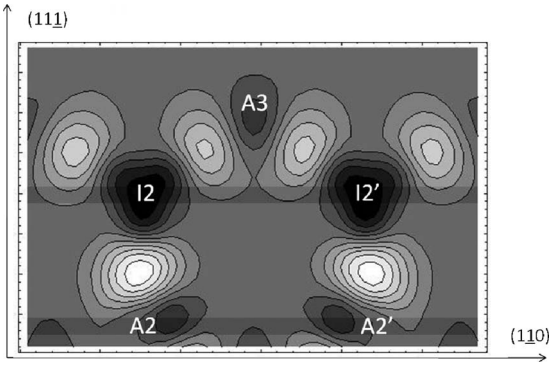

FIG. 12. Charge density difference between the adsorbate system and superposition of the clean silicon substrate and free indium atoms in a section of the surface unit cell. Light (dark) areas represent a positive (negative) difference. Atoms are labeled as in Fig. 8(a). Charge has been transferred into the region between the adsorbed indium atoms (I2, I2′) and the substrate silicon atoms (A2, A2′, A3). This suggests a covalent character of the bonds between substrate and adsorbed atoms. The peaks of the charge density difference are closer to silicon atoms due to their higher electronegativity.

VI. CONCLUSIONS

To understand the early stages of III-V epitaxy on a high index (112) surface of Si we investigate theoretically the atomic and electronic structure of submonolayer In coverage on that surface. Using *ab initio* calculations we compare two atomic models for the 7×1 indium-induced reconstruction observed on that surface. Based on the analysis of the adsorption energy and simulated STM images our results strongly support the substitutional model suggested by Gai and co-workers.[13] For this model the surface is found semiconducting. We also find that the work function is lowered by as much as 0.46 eV from the value calculated for the clean surface. In addition, we have performed a comprehensive theoretical study of the (112) surface of carbon diamond, silicon, germanium and α-tin. For Si we find the (1×1) rebonded reconstruction to be most stable. For carbon a (2×2) reconstruction is most favorable energetically, while the (2×1) reconstruction is only slightly higher in energy. Both tin and germanium prefer a (2×1) reconstruction. Surprisingly, in all cases, the driving force of reconstruction is dimerization, similar to that found, for example, for the (2×1)-reconstructed Si(001) surface. The electronic structure analysis reveals that in the case of Si and Ge all considered reconstructions are semiconducting. In the case of carbon the Fermi level is pinned by a surface state 1.5 eV above the valence band top. The calculated work functions vary from 5.17 to 4.46 eV when going form carbon to α-tin in good agreement with available experiment.

ACKNOWLEDGMENTS

We thank Michael Gerrity for his help in the early stages of this project. This work is supported by the National Science Foundation under Grant No. DMR-0548182 and the Texas Advanced Computing Center.

*demkov@physics.utexas.edu

[1] R. Droopad, K. Rajagopalan, J. Abrokwah, P. Zurcher, and M. Passlack, Microelectron. Eng. **84**, 2138 (2007).
[2] S. Datta, Microelectron. Eng. **84**, 2133 (2007).
[3] K. Eisenbeiser, R. Emrick, R. Droopad, Z. Yu, J. Finder, S. Rockwell, J. Holmes, C. Overgaard, and W. Ooms, IEEE Electron Device Lett. **23**, 300 (2002).
[4] P. N. Uppal and H. Kroemer, J. Appl. Phys. **58**, 2195 (1985).

[5] A. A. Stekolnikov, J. Furthmüller, and F. Bechstedt, Phys. Rev. B **65**, 115318 (2002).
[6] T. J. de Lyon, S. M. Johnson, C. A. Cockrum, O. K. Wu, W. J. Hamilton, and G. S. Kamath, J. Electrochem. Soc. **141**, 2888 (1994).
[7] M. Kawano, A. Ajisawa, N. Nagashima, and H. Wada, Appl. Phys. Lett. **69**, 2876 (1996).
[8] A. Million, N. K. Dhar, and J. H. Dinan, J. Cryst. Growth **159**, 76 (1996).
[9] S. Rujirawat, D. J. Smith, J. P. Faurie, G. Neu, V. Nathan, and S. Sivananthan, J. Electron. Mater. **27**, 1047 (1998).
[10] T. J. de Lyon, D. Rajavel, S. M. Johnson, and C. A. Cockrum, Appl. Phys. Lett. **66**, 2119 (1995).
[11] B. Yang, Y. Xin, S. Rujirawat, N. D. Browning, and S. Sivananthan, J. Appl. Phys. **88**, 115 (2000).
[12] E.-S. Cho, J.-W. Park, H. Hur, N.-H. Kim, J.-Y. Baik, C.-H. Jeon, C.-C. Hwang, K.-S. An, and C. Y. Park, Jpn. J. Appl. Phys., Part 1 **43**, 1312 (2004).
[13] Z. Gai, R. G. Zhao, W. S. Yang, and T. Sakurai, Phys. Rev. B **61**, 9928 (2000).
[14] S. C. Erwin, A. A. Baski, L. J. Whitman, and R. E. Rudd, Phys. Rev. Lett. **83**, 1818 (1999).
[15] S. M. Prokes and O. J. Glembocki, J. Vac. Sci. Technol. A **17**, 1410 (1999).
[16] A. A. Baski *et al.*, Surf. Sci. **423**, L265 (1999).
[17] A. A. Baski and L. J. Whitman, J. Vac. Sci. Technol. B **14**, 992 (1996).
[18] J. Kraft, M. G. Ramsey, and F. P. Netzer, Phys. Rev. B **55**, 5384 (1997).
[19] Xian-Qi Dai, Wei-Wei Ju, Guang-Tao Wang, and M. H. Xie, Surf. Sci. **572**, 77 (2004).
[20] P. Hohenberg and W. Kohn, Phys. Rev. **136**, B864 (1964); W. Kohn and L. J. Sham, Phys. Rev. **140**, A1133 (1965).
[21] P. E. Blöchl, Phys. Rev. B **50**, 17953 (1994).
[22] G. Kresse and D. Joubert, Phys. Rev. B **59**, 1758 (1999).
[23] G. Kresse and J. Furthmüller, Phys. Rev. B **54**, 11169 (1996); G. Kresse and J. Hafner, *ibid.* **47**, R558 (1993).
[24] H. J. Monkhorst and J. D. Pack, Phys. Rev. B **13**, 5188 (1976).
[25] C. Kittel, *Introduction to Solid State Physics*, 3rd. ed. (Wiley, New York, 1966), p. 29.
[26] B. Z. Olshanetsky and V. I. Mashanov, Surf. Sci. **111**, 414 (1981).
[27] S. L. Wright, H. Kroemer, and M. Inada, J. Appl. Phys. **55**, 2916 (1984).
[28] R. Kaplan, Surf. Sci. **116**, 104 (1982).
[29] Th. Berghaus, A. Brodde, H. Neddermeyer, and St. Tosch, Surf. Sci. **184**, 273 (1987).
[30] X. Wang and W. H. Weinberg, Surf. Sci. **314**, 71 (1994).
[31] A. A. Baski and L. J. Whitman, Phys. Rev. Lett. **74**, 956 (1995).
[32] A. A. Baski and L. J. Whitman, J. Vac. Sci. Technol. A **13**, 1469 (1995).
[33] A. A. Baski, S. C. Erwin, and L. J. Whitman, Science **269**, 1556 (1995).
[34] D. H. Zavitz, A. Evstigneeva, R. Singh, M. Trenary, and C. Fulk, J. Electron. Mater. **34**, 839 (2005).
[35] C. Fulk, S. Sivananthan, D. Zavitz, R. Singh, M. Trenary, Y. P. Chen, G. Brill, and N. Dhar, J. Electron. Mater. **35**, 1449 (2006).
[36] D. J. Chadi, Phys. Rev. B **29**, 785 (1984).
[37] D. J. Chadi and J. R. Chelikowsky, Phys. Rev. B **24**, 4892 (1981).
[38] C. H. Grein, J. Cryst. Growth **180**, 54 (1997).
[39] A. Mazur and J. Pollmann, Phys. Rev. B **30**, 2084 (1984).
[40] S. Mankefors, Surf. Sci. **443**, 99 (1999).
[41] D. M. Bylander and L. Kleinman, Phys. Rev. B **36**, 3229 (1987).
[42] C. G. Van de Walle and R. M. Martin, Phys. Rev. B **35**, 8154 (1987).
[43] J. van der Weide, Z. Zhang, P. K. Baumann, M. G. Wensell, J. Bernholc, and R. J. Nemanich, Phys. Rev. B **50**, 5803 (1994).
[44] W. Harrison, *Electronic Structure and the Properties of Solids* (Dover, New York, 1989).
[45] J. Pollmann and P. Krueger, *Handbook of Surface Science* (Elsevier, New York, 2000), Vol. 2, Chap. 2, p. 125.
[46] M. Scheffler and C. Stampfl, *Handbook of Surface Science* (Elsevier, New York, 2000), Vol. 2, Chap. 5, p. 294.
[47] J. Tersoff and D. R. Hamann, Phys. Rev. B **31**, 805 (1985).
[48] S.-H. Lee, W. Moritz, and M. Scheffler, Phys. Rev. Lett. **85**, 3890 (2000).
[49] G. P. Srivastava, *Theoretical Modelling of Semiconductor Surfaces—Microscopic Studies of Electrons and Phonons* (World Scientific, Singapore, 1999).